crystals

MDPI

Article

Anticancer Structure–Activity Relationship in Well-Characterized Pt(IV) Compounds: $Pt(CH_3)_2I_2${6,6′-dimethyl-2,2′-bipyridine} Cytotoxicity Against Colon and Ovarian Carcinoma Cell Lines

Shadrach Stitz [1], William A. Howard [1,*], Kraig A. Wheeler [2], Natarajan Ganesan [3] and David G. Churchill [4]

[1] Department of Chemistry & Biochemistry, University of Alaska Fairbanks, 1930 Yukon Drive, Fairbanks, AK 99775, USA; sjstitz@alaska.edu
[2] Department of Chemistry, Whitworth University, Spokane, WA 99251, USA; kraigwheeler@whitworth.edu
[3] College of Osteopathic Medicine, New York Institute of Technology, 504 University Loop, Jonesboro, AR 72401, USA; nganesan@nyit.edu
[4] Department of Chemistry (Molecular Logic Gate Laboratory), Korea Advanced Institute of Science and Technology, Building E6-4 (Room 5103), 373–1 Guseong–dong, Yuseong–gu, Daejeon 305-701, Republic of Korea; dchurchill@kaist.ac.kr
* Correspondence: wahoward@alaska.edu

Abstract

Well-defined, small-molecule, platinum-centered coordination compounds are of continued interest in both basic and applied research, particularly in medicinal chemistry and pharmaceuticals (i.e., cisplatin). Organoplatinum(IV) complexes have been reported to exhibit substantial in vitro cytotoxicity across a range of cancer cell lines. Compared with coordinatively unsaturated platinum(II) species, electronically and coordinatively saturated platinum(IV) complexes are generally more inert, reducing undesirable side reactions in plasma and cellular environments and potentially improving their safety profiles as chemotherapeutic agents. In addition, the presence of organic ligands can enhance lipophilicity, facilitating passive diffusion across cell membranes. Here, we report the synthesis, structural characterization, and in vitro anticancer activity of a series of organoplatinum(IV) complexes of the general formula $Pt(CH_3)_2I_2${n,n′-dimethyl-2,2′-bipyridine} (n,n′ = 4,4′; 5,5′; 6,6′). The 5,5′- and 6,6′-dimethyl isomers were characterized by single-crystal X-ray diffraction. All three dimethyl-substituted complexes, along with the parent compound, $Pt(CH_3)_2I_2${2,2′-bipyridine}, were evaluated for cytotoxic activity against a panel of 60 human cancer cell lines. Whereas $Pt(CH_3)_2I_2${2,2′-bipyridine} and the 4,4′- and 5,5′-dimethyl derivatives displayed limited cytotoxicity, the 6,6′-dimethyl isomer exhibited notable activity, particularly against the colon cancer cell line HCT-116 (LC_{50} = 8.17 μM) and the ovarian cancer cell line OVCAR-3 (LC_{50} = 7.34 μM). The enhanced cytotoxicity of the 6,6′-dimethyl derivative is attributed, at least in part, to the relatively facile dissociation of the 6,6′-dimethyl-2,2′-bipyridine ligand from the platinum(IV) center, suggesting that sterically induced ligand lability plays an important role in modulating biological activity in this particular compound, giving new structural activity impetus for potential drug molecules.

Keywords: platinum(IV); ovarian cancer; colon cancer; cytotoxicity study

Check for updates

Received: 16 March 2026
Revised: 2 April 2026
Accepted: 8 April 2026
Published: 14 April 2026

Copyright: © 2026 by the authors. Licensee MDPI, Basel, Switzerland. This article is an open access article distributed under the terms and conditions of the Creative Commons Attribution (CC BY) license.

1. Introduction

A number of organoplatinum(IV) complexes have been reported to be cytotoxic toward a variety of cancer cell lines [1–4]. Electronically and coordinatively saturated platinum(IV)

complexes tend to be more inert in plasma and cellular environments than are square planar, 16-electron platinum(II) complexes [5]. As a result, the platinum(IV) drugs undergo fewer unwanted side reactions with proteins. Furthermore, the organic ligands bonded to the platinum center impart lipophilicity to the drug, facilitating its diffusion through the cancer cell membrane [6]. Finally, many of the organoplatinum(IV) anticancer drugs possess multidentate ancillary ligands that further stabilize the drug [7].

The organoplatinum(IV) complexes $Pt(CH_3)_2X_2${4,4′-di-*tert*-butyl-2,2′-bipyridine} (X = Cl, Br) [8] exhibit potent cytotoxicity toward human breast cancer cells (cell line MCF-7) [9,10] and toward two leukemia cell lines (Jurkat [11,12] and K562 [13]). The unit cell of $Pt(CH_3)_2Br_2${4,4′-di-*tert*-butyl-2,2′-bipyridine} contains eight molecules [14]. The intermolecular distance between pyridine carbon atoms in two of these molecules is 3.474 Å, which is close to the sum of the van der Waals radii of two carbon atoms (ca. 3.40 Å) [15]. Thus, despite having two sterically demanding *tert*-butyl groups attached to the bipyridine ligand, the crystallographic evidence suggests that the coordinated 4,4′-di-*tert*-butyl-2,2′-bipyridine ligand is capable of intermolecular π–π interactions. Such interactions are important for driving the intercalation of some chemotherapy drugs into the major and/or minor grooves of tumor DNA [16–19]. Indeed, electronic absorption spectroscopy, circular dichroism spectroscopy, and fluorescence experiments provide evidence that both $Pt(CH_3)_2X_2${4,4′-di-*tert*-butyl-2,2′-bipyridine} (X = Cl, Br) complexes interact with DNA [8].

We have described the anticancer activity of $Pt(CH_3)_2I_2${2,2′-bipyridine} [20] against the human breast cancer cell line ZR-75-1 [21], and the anticancer activity of $[Pt(CH_3)_3]_2(\mu\text{-}I)_2$(μ-adenine) against various cell lines of non-small cell lung cancer, colon cancer, central nervous system cancer, melanoma, ovarian cancer, renal cancer, and triple negative breast cancer [22]. Given that both 2,2′-bipyridine and 4,4′-di(*tert*-butyl)-2,2′-bipyridine, when coordinated to a Pt(IV) center, can engage in intermolecular π–π interactions and possibly lead to intercalation between tumor DNA base pairs, we were curious as to how the steric demands of alkyl-substituted bipyridines might influence cytotoxicity. In this present work, we report the syntheses, structures, and anticancer activities of the series of compounds $Pt(CH_3)_2I_2${n,n′-$(CH_3)_2$-2,2′-bipyridine} where n,n′ = 4,4′; 5,5′; and 6,6′. This study revealed that the anticancer properties of these complexes depend significantly on which isomer of n,n′-$(CH_3)_2$-2,2′-bipyridine is used.

2. Experimental Details

General Considerations. Tetrahydrofuran, 4,4′-dimethyl-2,2′-bipyridine, 5,5′-dimethyl-2,2′-bipyridine, and 6,6′-dimethyl-2,2′-bipyridine were purchased from commercial suppliers and were used as received. Diiododimethylplatinum(IV) [23] and (2,2′-bipyridine)diiododimethylplatinum(IV) [20] were prepared by published procedures. Calf thymus DNA (sodium salt, Type I fibers) was purchased from Sigma-Aldrich (St. Louis, MO, USA). All ^{1}H and ^{13}C NMR spectra were obtained at room temperature on either a Varian Mercury 300 MHz FT-NMR spectrometer (Palo Alto, CA, USA) at the frequencies 300.068 MHz and 75.452 MHz, respectively, or a Bruker Ascend 600 MHz FT-NMR spectrometer (Billerica, MA, USA) running Topspin 3.6 at the frequencies 600.164 MHz and 150.925 MHz, respectively. ^{1}H and ^{13}C chemical shifts are reported in parts per million relative to the resonance for $SiMe_4$ (δ 0) and were referenced internally concerning the protio solvent impurity (δ 1.73 ppm and 3.58 ppm for THF-d_8; δ 2.75 ppm, 2.92 ppm, and 8.03 ppm for DMF-d_7) or the ^{13}C resonances (δ 25.37 ppm and 67.57 ppm for THF-d_8; δ 30.53 ppm, 35.66 ppm, and 163.15 ppm for DMF-d_7), respectively. ^{195}Pt NMR spectra were obtained at room temperature on a Bruker Ascend 600 MHz FT-NMR spectrometer running Topspin 3.6 at the frequency 129.015 MHz. In the ^{195}Pt NMR spectra, peaks were

referenced externally to a solution of K_2PtCl_4 in D_2O ($\delta = -1620$ ppm) [24]. Infrared spectra were recorded as KBr pellets on a Nicolet Magna-IR 560 spectrometer (Madison, WI, USA). Ultraviolet–visible absorption spectra were recorded on a Jasco V-730 spectrophotometer (Easton, MD, USA). Elemental analyses were carried out by Atlantic Microlab, Inc. (Norcross, GA, USA). Unless otherwise noted, all reactions and manipulations were carried out in the presence of air. All reagents and solvents were obtained from commercial suppliers and were used without further purification.

1. *Syntheses of the $Pt(CH_3)_2I_2${n,n′-$(CH_3)_2$-2,2′-bipyridine} Isomers.*

$Pt(CH_3)_2I_2${4,4′-$(CH_3)_2$-2,2′-bipyridine} shall be abbreviated as **4**;
$Pt(CH_3)_2I_2${5,5′-$(CH_3)_2$-2,2′-bipyridine}, as **5**;
$Pt(CH_3)_2I_2${6,6′-$(CH_3)_2$-2,2′-bipyridine}, as **6**.

A general synthetic procedure for compounds **4**, **5**, and **6** is as follows.

For **4** and **5**, an orange heterogeneous mixture of $[Pt(CH_3)_2I_2]_x$ (50.0 mg, 0.104 mmol) and an n,n′-$(CH_3)_2$-2,2′-bipyridine isomer (19.0 mg, 0.104 mmol) in tetrahydrofuran (8 mL) was stirred magnetically in a 50 mL, ChemGlass air-free storage vessel at 75 °C for 6 h. For **6**, the same procedure was carried out, but 61.0 mg (0.127 mmol) of $[Pt(CH_3)_2I_2]_x$ and 30.0 mg (0.163 mmol) of 6,6′-$(CH_3)_2$-2,2′-bipyridine were used.

In the case of compound **4**, the reaction mixture, appearing as a dull yellow suspension, was cooled to room temperature. The THF suspension was concentrated to a volume of approximately 0.5 mL by slow evaporation of the solvent at room temperature. The remaining THF supernatant was removed from the product, a dull greenish yellow powder, and the product was air-dried. Yield = 0.059 g (86%).

For products **5** and **6**, the orange homogeneous reaction mixtures were cooled to room temperature and concentrated to a volume of approximately 0.5 mL by slow evaporation at room temperature. Orange crystalline blocks of **5** and red crystalline blocks of **6** were found to have precipitated from the solutions. The crystals were then isolated and air-dried. Yield of **5** = 0.055 g (80%). Yield of **6** = 0.061 g (73%).

Anal. Calc. for $C_{14}H_{18}I_2N_2Pt$: C, 25.35%; H, 2.74%; N, 4.22%. For **4**, found: C, 25.72%; H, 2.53%; N, 4.22%. For **5**, found: C, 26.30%; H, 2.53%; N, 4.20%. For **6**, found: C, 25.83%; H, 2.55%; N, 4.16%. ^1H, ^{13}C, and ^{195}Pt NMR data for compounds **4**, **5**, and **6** are summarized in Table S1, and the infrared data are summarized in Table S2. Tables S1 and S2 as well as reproductions of all the NMR and infrared spectra are included in the Supplementary Information.

2. *Reactions Involving 2,2′-Bipyridine and **5** and **6**.*

A mixture of **5** (0.0050 g, 7.5 μmol) and 2,2′-bipyridine (0.0012 g, 7.7 μmol) in THF-d_8 (~0.75 mL) was created in an NMR tube. After 24 h at room temperature, ^1H NMR showed a mixture of only the starting materials in the solution.

A mixture of **6** (0.0050 g, 7.5 μmol) and 2,2′-bipyridine (0.0012 g, 7.7 μmol) in THF-d_8 (~0.75 mL) was created in an NMR tube. After 24 h at room temperature, ^1H NMR showed a mixture of only $Pt(CH_3)_2I_2${2,2′-bipyridine} [20] and free 6,6′-$(CH_3)_2$-2,2′-bipyridine in the NMR tube. Little to no unreacted **6** or 2,2′-bipyridine was found to be remaining.

3. *X-Ray Diffraction Studies*.

Orange blocks of **5** and red blocks of **6** were crystallized by the slow evaporation of the THF solvent from concentrated solutions at room temperature. X-ray intensity data were collected using a Bruker D8 Venture diffractometer (Billerica, MA, USA) equipped with a graphite monochromator and a Mo Kα microfocus INCOATEC Ims 3.0 sealed tube at 0.71073 Å. Data sets were corrected for Lorentz and polarization effects as well as absorption. The criterion for the observed reflections is $I > 2\sigma(I)$. Lattice parameters

were determined from least squares analysis and reflection data. Empirical absorption corrections were applied using SADABS [25]. The structure was solved by direct methods and refined by full-matrix least squares analysis of F^2 using X-Seed [26] equipped with SHELXT [27]. All non-hydrogen atoms were refined anisotropically by full-matrix least squares on F^2 using the SHELXL [27] program. Hydrogen atoms were included in idealized geometric positions with U_{iso} = 1.2 U_{eq} of the atom to which they are attached (U_{iso} = 1.5 U_{eq} for methyl groups). The hydrogen atoms attached to nitrogen or oxygen were located in difference maps and assigned 1.2 × U_{eq}. The frames were integrated with the Bruker SAINT software package version 8.40 using a narrow-frame algorithm. The structure was solved and refined using the Bruker SHELXTL software package version 2018/2, and the cell data and refinement parameters are summarized in Table 1.

Table 1. Crystal and intensity collection data for Products **5** and **6**.

Compound Number	**5**	**6**
chemical formula	$C_{14}H_{18}I_2N_2Pt$	$C_{14}H_{18}I_2N_2Pt$
molecular weight, g mol^{-1}	663.19	663.19
temperature, K	100 (2)	100 (2)
wavelength, Å	0.71073	0.71073
lattice	orthorhombic	orthorhombic
space group	Pbca	Pbca
cell constants		
a, Å	12.7995 (8)	14.7706 (10)
b, Å	14.4289 (10)	13.6001 (10)
c, Å	18.0758 (11)	16.4126 (12)
α, deg.	90	90
β, deg.	90	90
γ, deg.	90	90
volume, Å^3	3338.3 (4)	3297.0 (4)
Z	8	8
ρ (calc.) g cm^{-3}	2.639	2.672
absorption coefficient, mm^{-1}	12.095	12.247
F(000)	2400	2400
crystal size, mm^3	0.266 × 0.138 × 0.055	0.231 × 0.177 × 0.134
θ range	2.253 to 30.526°	2.384 to 30.564°
index ranges	−18 ≤ h ≤ +18 −20 ≤ k ≤ +20 −23 ≤ l ≤ +25	−19 ≤ h ≤ +21 −19 ≤ k ≤ +19 −23 ≤ l ≤ +23
reflections collected	111,168	60,295
independent reflections	5101 [R_{int} = 0.0626]	5039 [R_{int} = 0.0699]
coverage, independent reflections	99.9%	99.9%
absorption correction	Multi-scan	Multi-scan
max. and min. transmission	0.746 and 0.375	0.7461 and 0.2833

Table 1. *Cont.*

Compound Number	5	6
refinement method	Full matrix least squares on F^2	Full matrix least squares on F^2
data/restraints/parameters	5101/8/186	5039/0/176
goodness-of-fit on F^2	1.146	1.117
final *R* indices [I > 2σ(I)]	R_1 = 0.0208 wR_2 = 0.0475	R_1 = 0.0363 wR_2 = 0.0917
R indices (all data)	R_1 = 0.0245 wR_2 = 0.0486	R_1 = 0.0398 wR_2 = 0.0942
largest difference peak and hole	1.252 and −1.723 e $Å^{-3}$	2.542 and −4.484 e $Å^{-3}$

4. *Ultraviolet–Visible Absorption Studies.*

A stock solution was prepared by dissolving **6** in tetrahydrofuran (THF) to give a concentration of 10 mg mL^{-1} (≈15.1 mM) and stored at room temperature. Platinum working solutions (1 mM and 100 μM) were prepared by dilution of this stock solution with THF and were used for all binding experiments. Solutions of calf thymus DNA (ct-DNA, sodium salt, Type I fibers) were prepared at 1 mg mL^{-1} in 1× sodium saline citrate buffer (1× SSC). DNA fibers were allowed to dissolve overnight at 37 °C to ensure complete hydration. DNA concentration was determined spectrophotometrically using ε_{260} = 6600 M^{-1} cm^{-1} [28] and is reported in nucleotide phosphate (P) units. For binding studies, the DNA concentration was adjusted to 15 μg mL^{-1} (≈45 μM in P units), and this concentration was held constant while the platinum concentration was varied.

Aliquots of the platinum working solutions were added to the DNA solution to achieve phosphate-to-platinum (P/Pt) ratios of 40, 20, 10, 5, 2, and 1. The final platinum concentrations in the primary experiments were maintained at an absorbance within the linear range of the spectrophotometer and to facilitate accurate baseline correction. After mixing, samples were incubated for 30–60 min at room temperature prior to measurement. Electronic absorption spectra were recorded in 1 cm pathlength quartz cuvettes. Control spectra of ct-DNA alone (at the corresponding concentrations) and **6** alone (at matched concentrations in THF/SSC) were collected and used for baseline subtraction and comparison.

5. *In vitro Sulforhodamine B Assays.*

In vitro assays involving sixty human tumor cell lines were carried out by staff members in the National Cancer Institute's Developmental Therapeutics Program following a standardized procedure [29–31].

3. Results

$Pt(CH_3)_2I_2${4,4′-$(CH_3)_2$-2,2′-bipyridine} shall be abbreviated as **4**; $Pt(CH_3)_2I_2${5,5′-$(CH_3)_2$-2,2′-bipyridine}, as **5**; and $Pt(CH_3)_2I_2${6,6′-$(CH_3)_2$-2,2′-bipyridine}, as **6**. Products **4**, **5**, and **6** are formed by the reaction between the Lewis acid $[Pt(CH_3)_2I_2]_x$ and the appropriate dimethyl-bipyridine isomer. While **4** was insoluble in THF, **5** and **6** were both soluble. Products **5** and **6** were structurally characterized by single-crystal X-ray diffraction. Figure 1 shows the thermal ellipsoid plots (each 50% probability) of **5** and **6** with the non-hydrogen atoms labeled. Table 1 shows the crystal and intensity collection data, whereas Table 2 shows select metrical data for both complexes.

Bond distances and bond angles found in **5** are very similar to the corresponding bond distances and bond angles in **6**, and to those in $Pt(CH_3)_2I_2${2,2′-bipyridine} and in $Pt(CH_3)_2I_2${4,4′-$(CO_2H)_2$-2,2′-bipyridine} [20]. In the structure of **5**, there was evidence of some degree of crystallographic disorder. The atom in the position of C(14) refined as a carbon atom (96%) and as an iodine atom (4%), resulting from co-crystallization

with an isomer in which the two iodo ligands are *cis* to one another. Interestingly, such co-crystallization was not observed in the structures of **6**, $Pt(CH_3)_2I_2${2,2′-bipyridine}, or $Pt(CH_3)_2I_2${4,4′-$(CO_2H)_2$-2,2′-bipyridine} [20].

Table 2. Select metrical data (Å, deg.) for **5** and **6**.

Compound Number	5	6
Bond Lengths (Å)		
Pt–I(1)	2.6500 (3)	2.6453 (4)
Pt–I(2)	2.6429 (3)	2.6634 (4)
Pt–I(3)	2.539 (8)	
Pt–C(13)	2.064 (3)	2.063 (5)
Pt–C(14)	2.065 (5)	2.058 (5)
Pt–C(14A)	2.065 (5)	
Pt–N(1)	2.154 (3)	2.200 (4)
Pt–N(2)	2.163 (2)	2.218 (4)
Bond Angles (deg.)		
I(1)–Pt–I(2)	178.905 (8)	177.727 (13)
C(13)–Pt–N(2)	174.38 (12)	173.95 (19)
C(14)–Pt–N(1)	176.15 (16)	173.93 (19)
I(1)–Pt–C(13)	90.38 (11)	86.60 (16)
I(1)–Pt–C(14)	89.26 (15)	87.90 (15)
I(1)–Pt–N(1)	90.29 (7)	87.77 (11)
I(1)–Pt–N(2)	91.81 (7)	88.36 (10)
C(13)–Pt–C(14)	85.83 (17)	83.8 (2)
C(13)–Pt–N(1)	98.00 (11)	100.2 (2)
C(14)–Pt–N(2)	99.37 (16)	99.34 (18)
N(1)–Pt–N(2)	76.82 (10)	76.29 (15)
Pt–N(1)–C(5)	115.33 (19)	110.7 (3)
Dihedral Angle (deg.)		
N(1)–C(5)–C(6)–N(2)	−2.5 (4)	5.8 (6)
Pt–N(1)–C(1)–C(2)	−178.6 (2)	162.0 (4)

The unit cell of **5** contains eight molecules, and the closest intermolecular distance between the aromatic carbon atoms of one molecule and the aromatic carbon atoms in another is ca. 3.59 Å, which is very close to the sum of the van der Waals radii of two carbon atoms (ca. 3.40 Å) [15]. Thus, there may be some weak intermolecular π–π interactions in the unit cell of **5**. Similarly, the unit cell of **6** contains eight molecules, and the closest intermolecular distance between the aromatic carbon atoms of one molecule and the aromatic carbon atoms in another is ca. 3.58 Å. There may be weak intermolecular π–π interactions in the unit cell of **6** as well. If **5** and **6** are capable of intermolecular π–π interactions in their unit cells, then it seems reasonable to propose that these complexes may also engage in intermolecular π–π interactions with the nucleobases of tumor DNA.

An alternative view of the thermal ellipsoid plot of **6** is shown in Figure 2. This view clearly shows that the bipyridine plane is not coplanar with the plane defined by the platinum atom and the two nitrogen atoms. Indeed, the Pt–N(1)–C(1)–C(2) dihedral

angle is ca. 162.0°, a full 18.0° from co-planarity (for comparison, the same dihedral angle in **5** is nearly planar at −178.6°). Unfavorable steric interactions between the methyl groups attached to platinum and the methyl groups attached to bipyridine are most likely responsible for distorting the coordination of the 6,6′-$(CH_3)_2$-2,2′-bipyridine ligand. The distances between C(12) and C(14) and between C(11) and C(13) are 3.220 Å and 3.178 Å, respectively. Both distances are within the sum of the van der Waals radii of two carbon atoms (ca. 3.40 Å) [15], which supports the notion that steric repulsions exist between these respective methyl groups. Interestingly, the intramolecular, non-bonding distance between C(14) and C(13) is 2.752 Å in **6** and 2.811 Å in **5**.

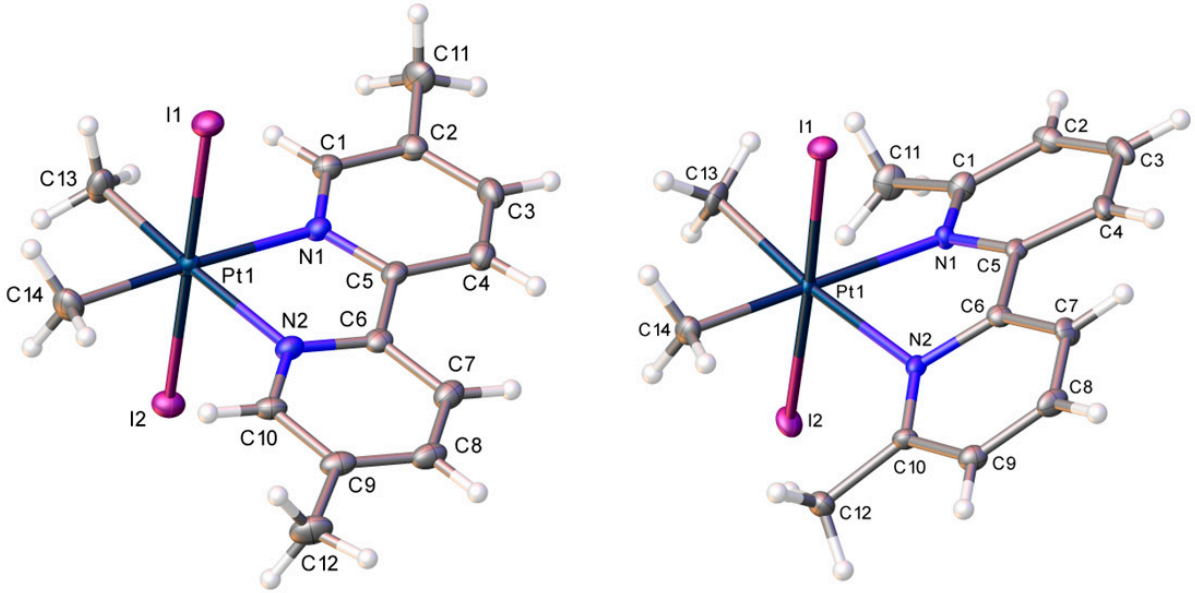


Figure 1. Thermal ellipsoid plots (each 50%) from the X-ray structures of $Pt(CH_3)_2I_2${5,5′-$(CH_3)_2$-2,2′-bipyridine} (**5**) (**left**) and $Pt(CH_3)_2I_2${6,6′-$(CH_3)_2$-2,2′-bipyridine} (**6**) (**right**). The minor disorder component of 5 has been omitted for clarity.

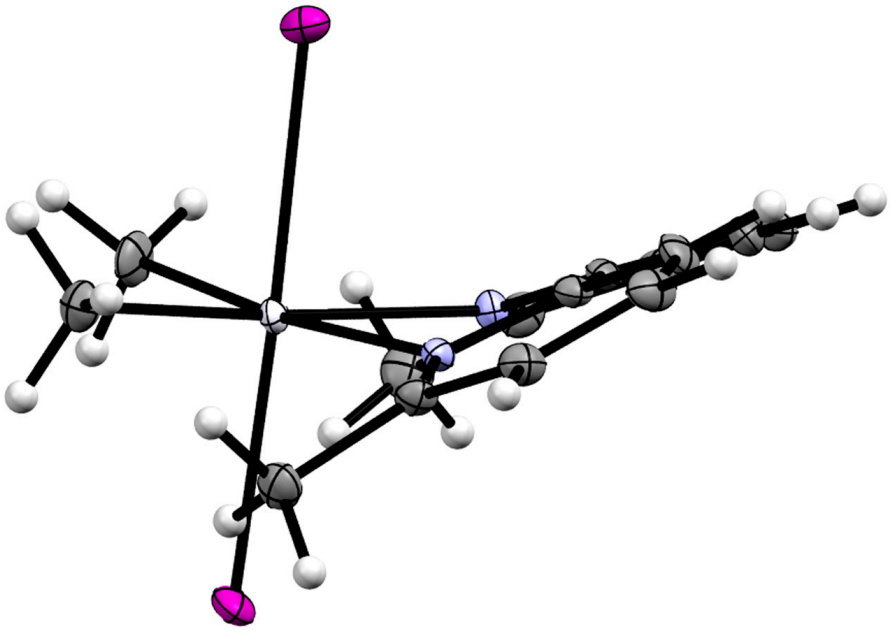


Figure 2. Alternative view of the thermal ellipsoid plot of **6**, showing the distortion of the coordinated 6,6′-$(CH_3)_2$-2,2′-bipyridine ligand.

The steric repulsions involving the methyl groups in **6** imply that the 6,6′-$(CH_3)_2$-2,2′-bipyridine ligand does not bond to the platinum(IV) center as strongly as 2,2′-bipyridine does, or as the other dimethyl-bipyridine ligands do. Indeed, as shown in Table 2, the Pt–N bond distances in **6** are slightly longer than those in **5**. The weaker coordination of the 6,6′-$(CH_3)_2$-2,2′-bipyridine ligand suggests that this ligand can dissociate from the platinum center. To test for ligand dissociation, **6** underwent reaction with one equivalent of 2,2′-bipyridine in THF-d_8 solution, as shown in Figure 3. ^{1}H NMR spectroscopy revealed that **6** reacts with 2,2′-bipyridine to form a mixture of $Pt(CH_3)_2I_2${2,2′-bipyridine} [20] and free 6,6′-$(CH_3)_2$-2,2′-bipyridine. The reaction was complete within 24 h at room temperature. Analysis by ^{1}H NMR spectroscopy also revealed that there is no chemical reaction between **5** and 2,2′-bipyridine in THF-d_8 solution after 24 h at room temperature.

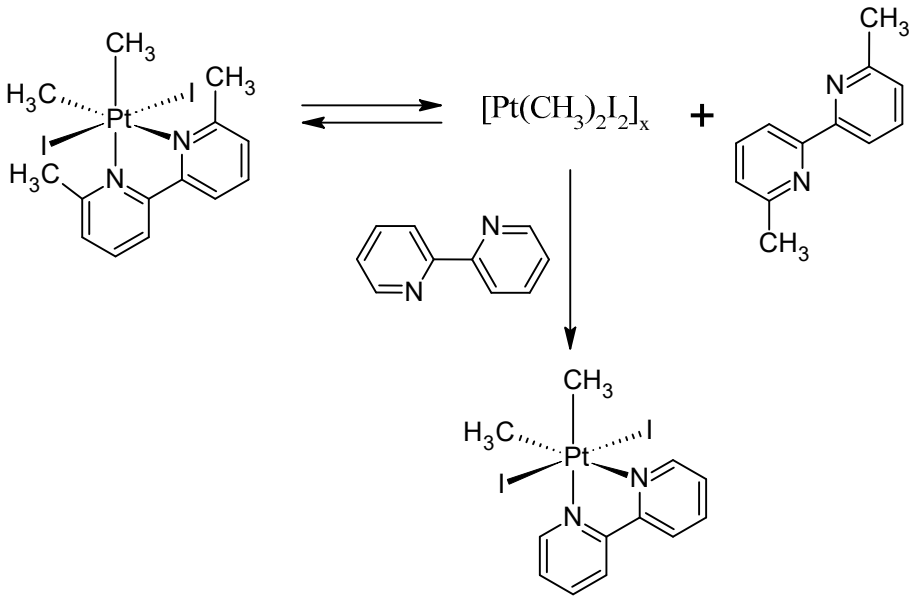


Figure 3. Reaction between **6** and 2,2′-bipyridine.

Given that the 6,6′-dimethyl-2,2′-bipyridine ligand dissociates from the platinum center more readily than the other bipyridine ligands examined in this study, complex **6** may interact with tumor cell DNA through a distinct mechanism. To investigate this possibility, the interaction of **6** with calf thymus DNA (ct-DNA) was evaluated by ultraviolet–visible absorption spectroscopy. A representative portion of the electronic absorption spectra recorded at varying DNA:**6** ratios is shown in Figure 4.

DNA base pairs exhibit a characteristic absorption band at 260 nm ($\varepsilon = 6600\ M^{-1}\ cm^{-1}$) [28]. As the DNA:**6** ratio decreases, a progressive increase in absorbance at this wavelength is observed. This hyperchromic effect [32] is consistent with disruption of the native double-helical structure, leading to partial strand unwinding and increased exposure of nucleobases to ultraviolet radiation. These results indicate that complex **6** interacts directly with DNA. The spectrum obtained at a DNA:**6** ratio of 1:1 exhibits a bathochromic shift of less than 1 nm relative to DNA alone, which suggests that intercalation of **6** with the nucleobases is unlikely [33].

Compounds **4**, **5**, **6**, and $Pt(CH_3)_2I_2${2,2′-bipyridine} were submitted to the National Cancer Institute's Developmental Therapeutics Program (NCI/DTP) for in vitro cell viability assays using their panel of 60 human cancer cell lines. These 60 cell lines consisted of 6 breast, 6 central nervous system, 7 colon, 6 leukemia, 9 melanoma, 9 non-small cell lung, 7 ovarian, 2 prostate, and 8 renal cancer cell lines. NCI typically runs a one-dose test first, in order to determine whether there is any anticancer activity at all against any of the 60 cell lines. If an experimental drug shows some appreciable anticancer activity,

then that drug is selected for further testing in a five-dose trial. In the five-dose trial only, three important parameters are measured: (a) the lethal concentration needed to kill 50% of the cancer cells (LC_{50}), (b) the drug concentration needed to cause 50% growth inhibition (GI_{50}), and (c) the concentration of drug needed for total growth inhibition (TGI).

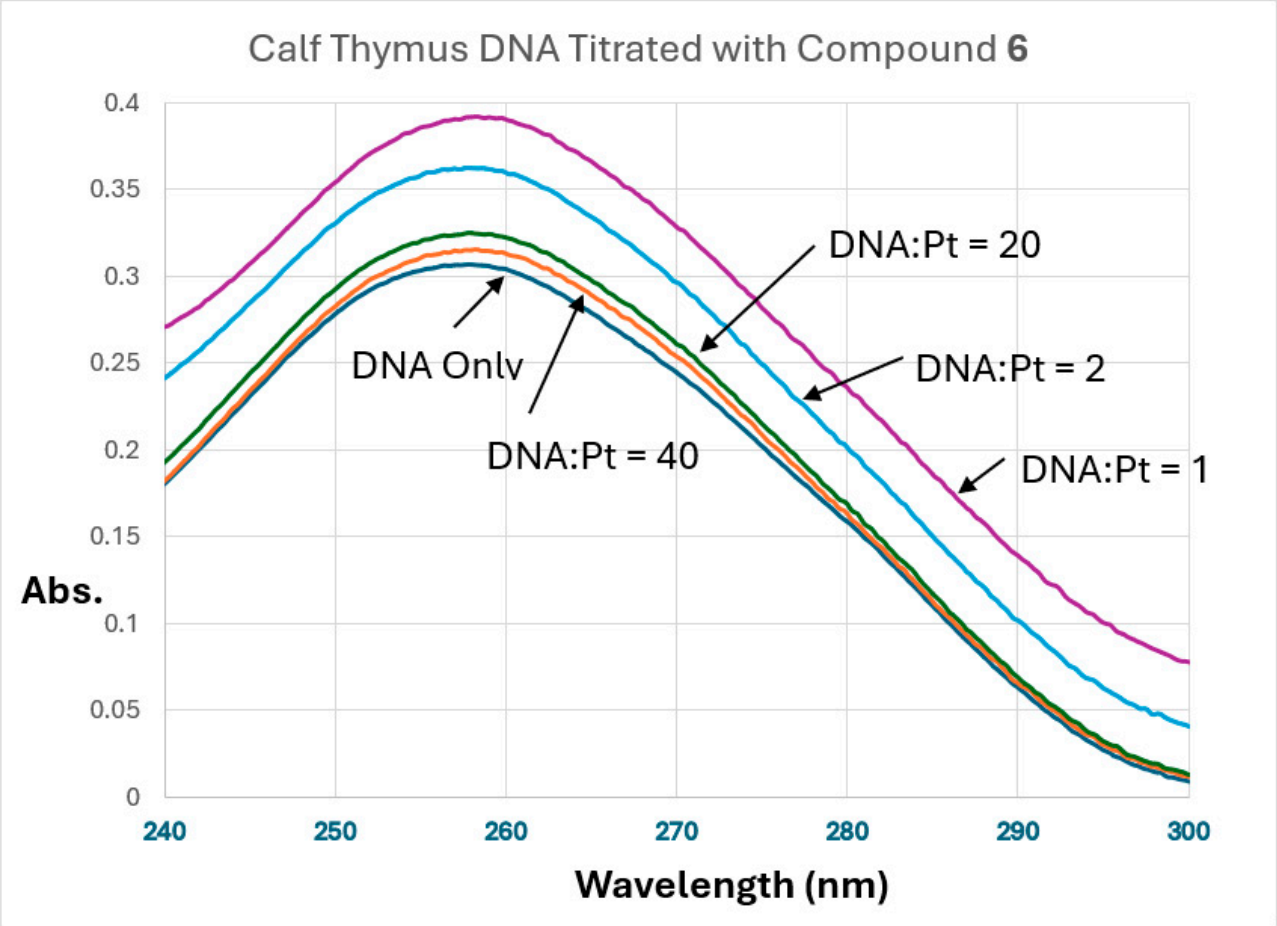


Figure 4. Electronic absorption spectrum, from 240 to 300 nm, of calf thymus DNA titrated with compound **6**, clearly showing a hyperchromic effect.

Compounds **4** and **5** were not selected for the five-dose test due to low cytotoxicity toward all 60 cell lines. Although we previously found that $Pt(CH_3)_2I_2\{2,2'$-bipyridine$\}$ was more cytotoxic than cisplatin against the human breast cancer cell line ZR-75-1 [20], this compound was not sufficiently active in the NCI assay to be selected for the five-dose test. Among the compounds tested here, only **6** was sufficiently active to be selected for the five-dose assay. Those assays in which **6** showed some cytotoxicity are summarized in Table 3. For comparison, the results involving cisplatin against the same cell lines are also included in Table 3, as values in parentheses.

Compound **6** was especially cytotoxic toward colon cancer cell line HCT-116 [34] (LC_{50} = 8.17 μM) but completely inactive toward the other colon cancer cell lines COLO-205 [35], HCC-2998 [36], HCT-15 [37], HT29 [38], KM12 [39], and SW-620 [40], with LC_{50} values > 100 μM in each case. HCT-116, HCT-15, and KM12 cells are high-frequency microsatellite unstable with impaired DNA mismatch repair [41], while the other colon cancer cell lines are microsatellite stable with proficient mismatch repair. HCT-116 differs from HCT-15 and KM12 in that the high-frequency microsatellite instability arises from biallelic Mut L Homolog 1 promoter methylation [42].

Table 3. In vitro cytotoxicity of **6** and cisplatin (values in parentheses) against some human cancer cell lines.

Cell Line, Reference	Type of Cancer	GI_{50}, μM	TGI, μM	LC_{50}, μM
CCRF-CEM, [43]	Leukemia	5.42 (1.47)	18.0 (>100)	42.5 (>100)
HL-60(TB), [44]	Leukemia	3.98 (4.12)	16.0 (75.1)	40.5 (>100)
K-562, [13]	Leukemia	4.62	19.3	60.2
MOLT-4, [45]	Leukemia	5.53 (2.75)	18.0 (>100)	42.8 (>100)
RPMI-8226, [46]	Leukemia	2.50 (6.44)	11.2 (>100)	33.6 (>100)
SR, [47]	Leukemia	4.19 (0.496)	16.2 (16.0)	40.5 (>100)
EKVX, [48]	Non-Small Cell Lung	1.41 (6.54)	4.52 (62.9)	79.5 (>100)
HOP-62, [31]	Non-Small Cell Lung	3.40 (1.54)	18.4 (13.2)	82.2 (>100)
NCI-H226, [49]	Non-Small Cell Lung	10.1 (4.42)	29.0 (25.6)	83.1 (>100)
NCI-H460, [50]	Non-Small Cell Lung	8.75 (0.455)	22.7 (78.2)	53.4 (>100)
NCI-H522, [51]	Non-Small Cell Lung	3.05	16.5	41.2
HCT-116, [34]	Colon Cancer	1.79 (9.24)	3.83 (>100)	**8.17** (>100)
SF-539, [52]	Central Nervous System	7.93 (0.600)	23.6 (7.67)	58.9 (>100)
U251, [53]	Central Nervous System	11.6 (1.57)	26.0 (24.7)	58.5 (>100)
SK-MEL-2, [54]	Melanoma	2.54	11.6	50.9
UACC-62, [55]	Melanoma	6.77 (1.34)	22.9 (9.39)	60.1 (37.2)
IGROV-1, [56]	Ovarian Cancer	2.07 (1.70)	5.10 (7.05)	42.6 (>100)
OVCAR-3, [57]	Ovarian Cancer	1.69 (1.93)	3.52 (4.27)	**7.34**
OVCAR-8, [58]	Ovarian Cancer	12.3 (4.09)	29.1 (>100)	68.7 (>100)
PC-3, [59]	Prostate Cancer	2.53 (4.08)	7.82 (>100)	73.0 (>100)
MCF-7, [9,10]	Breast Cancer	4.24 (2.66)	19.5 (79.3)	91.5 (>100)
BT-549, [60]	Breast Cancer	13.7 (3.36)	32.5 (44.9)	77.0 (>100)

Compound **6** was also especially cytotoxic toward ovarian cancer cell line OVCAR-3 [57] and displayed more limited activity toward the ovarian cancer cell lines OVCAR-8 [58] and IGROV-1 [56]. Compound **6** was inactive toward the ovarian cancer cell lines OVCAR-4 [61], OVCAR-5 [61], NCI/ADR-RES [62], and SKOV-3 [54]. OVCAR-3 and OVCAR-8 are high-grade serous ovarian cancer cells deficient in DNA repair made possible by homologous recombination [63]. Although IGROV1 cells have a BRCA1 mutation, their homologous recombination mechanism is proficient [64].

4. Discussion

The 6,6′-dimethyl-2,2′-bipyridine ligand in **6** dissociates from the platinum center and can be displaced by an alternative bidentate donor. This substitution behavior suggests that ligand dissociation is certainly feasible in a cellular environment. Accordingly, **6** is more appropriately regarded as a platinum(IV) prodrug rather than an intrinsically active chemotherapy drug.

To evaluate this hypothesis further, a trial reaction between **6** and one equivalent of glutathione was conducted in a 1:1 (*v*/*v*) THF-d_8/D_2O mixture. After incubation for 24 h at 37 °C, analysis by ^{1}H NMR spectroscopy confirmed that a chemical reaction had occurred. The spectrum displayed signals corresponding to unreacted **6** and a single, as yet unidentified product in approximately a 1:1 ratio. Notably, free 6,6′-dimethyl-2,2′-

bipyridine was not detected. Isolation and structural characterization of the product were not pursued, as the objective of this preliminary experiment was solely to determine whether reaction with glutathione would occur. A more comprehensive investigation of the reactivity of **6** and $[Pt(CH_3)_2I_2]_x$ toward glutathione will be reported separately.

6 demonstrably interacts with DNA, indicating that it may exert genotoxic effects in cancer cells. However, the propensity of the 6,6′-dimethyl-2,2′-bipyridine ligand to dissociate from the platinum center suggests that **6** is capable of engaging in additional substitution reactions with other intracellular nucleophiles. Consequently, its cytotoxic activity is unlikely to arise solely from DNA damage. Rather, the biological effects of **6** arise plausibly from the molecule engaging in both genotoxic and non-genotoxic pathways.

Cell viability assays conducted by the National Cancer Institute (Bethesda, MD, USA) demonstrated that **6** exhibits pronounced cytotoxicity toward the human colon cancer cell line HCT-116 and the high-grade serous ovarian cancer cell line OVCAR-3. Both lines are characterized by defects in DNA repair pathways: HCT-116 is deficient in mismatch repair, whereas OVCAR-3 exhibits impaired homologous recombination. However, compromised DNA repair alone does not fully account for the observed activity profile, as several other repair-deficient cell lines displayed minimal or no sensitivity to **6**. Notably, **6** produced lower LC_{50} values than cisplatin in all but one assay, the melanoma cell line UACC-62. Collectively, these data suggest that, while DNA repair deficiencies may contribute to susceptibility, additional determinants likely influence the cytotoxic response to **6**.

5. Conclusions

The anticancer activity of platinum iodide complexes is well-documented [65]. The four organoplatinum(IV)-iodide complexes $Pt(CH_3)_2I_2${2,2′-bipyridine}, $Pt(CH_3)_2I_2${4,4′-dimethyl-2,2′-bipyridine} (**4**), $Pt(CH_3)_2I_2${5,5′-dimethyl-2,2′-bipyridine} (**5**), and $Pt(CH_3)_2I_2${6,6′-dimethyl-2,2′-bipyridine} (**6**) were synthesized, isolated, and comprehensively characterized. Samples of each compound were subsequently submitted to the National Cancer Institute's Developmental Therapeutics Program for in vitro evaluation using the 60–human cancer cell line screening panel. In the initial single-dose screen, the first three complexes—those bearing unsubstituted, 4,4′-dimethyl-, and 5,5′-dimethyl-2,2′-bipyridine ligands—did not demonstrate sufficient antiproliferative activity to warrant progression to the five-dose assay. In contrast, **6** met the criteria for further evaluation and was advanced to the full five-dose screen. This analysis revealed pronounced cytotoxicity against the colon carcinoma cell line HCT-116 and the high-grade serous ovarian carcinoma cell line OVCAR-3. The enhanced cytotoxic activity of **6** is most plausibly attributed to the comparatively labile 6,6′-dimethyl-2,2′-bipyridine ligand, whose steric encumbrance likely facilitates dissociation from the platinum(IV) center, thereby promoting the formation of biologically active species.

Supplementary Materials: The following supporting information can be downloaded at: https://www.mdpi.com/article/10.3390/cryst16040263/s1, Figure S1: Full ^{1}H NMR spectrum of $Pt(CH_3)_2I_2${4,4′-dimethyl-2,2′-bipyridine: (**4**), Solvent = DMF-d_7; Figure S2: Portion of the ^{1}H NMR spectrum of **4**, showing only those peaks representing the methyl groups, DMF-d_7 and protonated DMF peaks also visible, Solvent = DMF-d_7; Figure S3: Portion of the ^{1}H NMR spectrum of **4**, showing only those peaks for H atoms bonded to the bipyridine rings, DMF peaks also visible, Solvent = DMF-d_7; Figure S4: Full ^{195}Pt NMR spectrum of $Pt(CH_3)_2I_2${4,4′-dimethyl-2,2′-bipyridine} (4), Solvent = DMF-d_7; Figure S5: Full ^{1}H NMR spectrum of $Pt(CH_3)_2I_2${5,5′-dimethyl-2,2′-bipyridine: (**5**), Solvent = THF-d_8; Figure S6: Portion of the ^{1}H NMR spectrum of **5**, showing only those peaks representing the methyl groups, THF-d_8 and small unidentified impurity peaks also visible, Solvent = THF-d_8; Figure S7: Portion of the ^{1}H NMR spectrum of **5**, showing only those peaks for H atoms bonded to the bipyridine rings, Solvent = THF-d_8; Figure S8: Full ^{13}C{^{1}H} NMR spectrum of $Pt(CH_3)_2I_2${5,5′-

dimethyl-2,2′-bipyridine} (**5**), Solvent = THF-d_8; Figure S9: Portion of the ^{13}C NMR spectrum of **5**, showing only those peaks representing the methyl groups, Solvent = THF-d_8; Figure S10: Portion of the ^{13}C NMR spectrum of **5**, showing only the aromatic carbons, Solvent = THF-d_8; Figure S11: Full ^{195}Pt NMR spectrum of $Pt(CH_3)_2I_2${5,5′-dimethyl-2,2′-bipyridine} (**5**), Solvent = THF-d_8; Figure S12: Full ^{1}H NMR spectrum of $Pt(CH_3)_2I_2${6,6′-dimethyl-2,2′-bipyridine} (**6**), Solvent = THF-d_8; Figure S13: Portion of the ^{1}H NMR spectrum of **6**, showing only those peaks representing the methyl groups, THF-d_8 and small unidentified impurity peaks also visible, Solvent = THF-d_8; Figure S14: Portion of the ^{1}H NMR spectrum of **6**, showing only those peaks for H atoms bonded to the bipyridine rings, Solvent = THF-d_8; Figure S15: Full ^{13}C{^{1}H} NMR spectrum of $Pt(CH_3)_2I_2${6,6′-dimethyl-2,2′-bipyridine} (**6**), Solvent = THF-d_8; Figure S16: Portion of the ^{13}C NMR spectrum of **6**, showing only those peaks representing the methyl groups, Solvent = THF-d_8; Figure S17: Portion of the ^{13}C NMR spectrum of **6**, showing only the aromatic carbons, Solvent = THF-d_8; Figure S18: Full ^{195}Pt NMR spectrum of $Pt(CH_3)_2I_2${6,6′-dimethyl-2,2′-bipyridine} (**6**), Solvent = THF-d_8; Figure S19: Infrared spectrum of **4** (KBr pellet); Figure S20: Infrared spectrum of **5** (KBr pellet); Figure S21: Infrared spectrum of **6** (KBr pellet); Table S1: NMR spectroscopic data for products **4**, **5**, and **6**; Table S2: Infrared absorption data (cm^{-1}, KBr pellets), vs = very strong absorption, s = strong absorption, m = medium intensity absorption, w = weak absorption; Ultraviolet-visible spectroscopy study of the interaction of compound **6** with calf thymus DNA, experimental details and raw absorption data; In vitro cell viability assays, National Cancer Institute Devlopmental Therapeutics Program 60 Cell Panel, raw data; X-ray CheckCIF reports.

Author Contributions: Conceptualization, writing, project administration, W.A.H.; synthesis, spectroscopic characterization, S.S.; ultraviolet–visible absorption study, N.G.; X-ray crystallography, K.A.W.; writing and experimental designs, D.G.C. All authors have read and agreed to the published version of the manuscript.

Funding: This research received no external funding.

Data Availability Statement: Crystallographic data have been deposited with the Cambridge Crystallographic Data Centre, under deposition numbers 2533373 (compound **5**) and 2533374 (compound **6**). These data can be obtained free of charge at https://www.ccdc.cam.ac.uk/ or from the Cambridge Crystallographic Data Centre, 12, Union Road, Cambridge CB2 1EZ, UK; email: deposit@ccdc.cam.ac.uk; fax +44 (0)1223-336408. Any other data are available on request from the corresponding author.

Acknowledgments: The authors thank the Department of Chemistry & Biochemistry at the University of Alaska Fairbanks (UAF) for financial support of this work. At UAF, the 600 MHz NMR spectrometer was purchased with funding from the US Army Medical Research and Material Command (05178001), and the 300 MHz NMR spectrometer was purchased with funding from the National Science Foundation (DUE−9850731). Support for maintaining the 600 MHz NMR spectrometer at UAF was supplied by an Institutional Development Award (IDeA) from the National Institute of General Medical Sciences of the National Institutes of Health (NIH) under grant number P20GM103395. S.S. received support from the BLaST Program, which is supported by the NIH Common Fund, through the Office of Strategic Coordination, Office of the NIH Director, with the linked awards: TL4GM118992, RL5GM118990, and UL1GM118991. The content is solely the responsibility of the authors and does not necessarily reflect the official views of the NIH. UAF is an affirmative action/equal employment opportunity employer and educational institution: https://www.alaska.edu/nondiscrimination/ (access on 10 April 2026).) The National Science Foundation's Major Research Instrumentation is acknowledged for their support (1827313) in the purchase of the Bruker D8 Venture X-ray diffractometer at Whitworth University. The authors thank the National Cancer Institute Developmental Therapeutics Program (NCI/DTP) and acknowledge NCI/DTP (https://dtp.cancer.gov) for providing the in vitro sulforhodamine B assay data for $Pt(CH_3)_2I_2${6,6′-dimethyl-2,2′-bipyridine} (NSC 855004/1) and cisplatin (NSC 119875/97). DGC acknowledges KAIST and the KC30 program at KAIST.

Conflicts of Interest: The authors declare no conflicts of interest.

References

1. Escolà, A.; Crespo, M.; López, C.; Quirante, J.; Jayaraman, A.; Polat, I.H.; Badía, J.; Baldomà, L.; Cascante, M. On the Stability and Biological Behavior of Cyclometallated Pt(IV) Complexes with Halido and Aryl Ligands in the Axial Positions. *Bioorg. Med. Chem.* **2016**, *24*, 5804–5815. [CrossRef]
2. Tan, M.-X.; Wang, Z.-F.; Qin, Q.-P.; Huang, X.-L.; Zou, B.-Q.; Liang, H. Complexes of Platinum(II/IV) with 2-Phenylpyridine Derivatives as a New Class of Promising Anticancer Agents. *Inorg. Chem. Commun.* **2019**, *108*, 107510. [CrossRef]
3. Annunziata, A.; Amoresano, A.; Cucciolito, M.E.; Esposito, R.; Ferraro, G.; Iacobucci, I.; Imbimbo, P.; Lucignano, R.; Melchiorre, M.; Monti, M.; et al. Pt(II) Versus Pt(IV) in Carbene Glycoconjugate Antitumor Agents: Minimal Structural Variations and Great Performance Changes. *Inorg. Chem.* **2020**, *59*, 4002–4014. [CrossRef] [PubMed]
4. Bauer, E.; Domingo, X.; Balcells, C.; Polat, I.H.; Crespo, M.; Quirante, J.; Badía, J.; Baldomà, L.; Font-Bardia, M.; Cascante, M. Synthesis, Characterization and Biological Activity of New Cyclometallated Platinum(IV) Iodido Complexes. *Dalton Trans.* **2017**, *46*, 14973–14987. [CrossRef]
5. Johnston, T.C.; Suntharalingam, K.; Lippard, S.J. The Next Generation of Platinum Drugs: Targeted Pt(II) Agents, Nanoparticle Delivery, and Pt(IV) Prodrugs. *Chem. Rev.* **2016**, *116*, 3436–3486. [CrossRef] [PubMed]
6. Ghezzi, A.R.; Aceto, M.; Cassino, C.; Gabano, E.; Osella, D. Uptake of Antitumor Platinum(II)-Complexes by Cancer Cells, Assayed by Inductively Coupled Plasma Mass Spectrometry (ICP-MS). *J. Inorg. Biochem.* **2004**, *98*, 73–78. [CrossRef] [PubMed]
7. Crespo, M. Cyclometallated Platinum(IV) Compounds as Promising Antitumour Agents. *J. Organomet. Chem.* **2019**, *879*, 15–26. [CrossRef]
8. Pouryasin, Z.; Yousefi, R.; Nabavizadeh, S.M.; Rashidi, M.; Hamidizadeh, P.; Alavianmehr, M.-M.; Moosavi-Movahedi, A.A. Anticancer and DNA Binding Activities of Platinum(IV) Complexes: Importance of Leaving Group Departure Rate. *Appl. Biochem. Biotechnol.* **2014**, *172*, 2604–2617. [CrossRef]
9. Levenson, A.S.; Jordan, V.C. MCF-7: The First Hormone-Responsive Breast Cancer Cell Line. *Cancer Res.* **1997**, *57*, 3071–3078.
10. Lee, A.V.; Oesterreich, S.; Davidson, N.E. MCF-7 Cells—Changing the Course of Breast Cancer Research and Care for 45 Years. *J. Natl. Cancer Inst.* **2015**, *107*, djv073. [CrossRef]
11. Schneider, U.; Schwenk, H.-U.; Bornkamm, G. Characterization of EVB-Genome Negative "Null" and "T" Cell Lines Derived from Children with Acute Lymphoblastic Leukemia and Leukemic Transformed Non-Hodgkin Lymphoma. *Int. J. Cancer* **1977**, *19*, 621–626. [CrossRef] [PubMed]
12. Schwenk, H.-U.; Schneider, U. Cell Cycle Dependency of a T Cell Marker on Lymphoblasts. *Blut Zeit. Gesamte Blutforsch.* **1975**, *31*, 299–306. [CrossRef] [PubMed]
13. Lozzio, C.B.; Lozzio, B.B. Human Chronic Myelogenous Leukemia Cell-Line with Positive Philadelphia Chromosome. *Blood* **1975**, *45*, 321–334. [CrossRef] [PubMed]
14. Kelly, M.E.; Gómez-Ruiz, S.; Kluge, R.; Merzweiler, K.; Steinborn, D.; Wagner, C.; Schmidt, H. Studies of Mononuclear and Dinuclear Complexes of Dibromodimethylplatinum(IV): Preparation, Characterization and Crystal Structures. *Inorg. Chim. Acta* **2009**, *362*, 1323–1332. [CrossRef]
15. Batsanov, S.S. Van der Waals Radii of Elements. *Inorg. Mater.* **2001**, *37*, 1031–1046. [CrossRef]
16. Zamora, A.; Wachter, E.; Vera, M.; Heidary, D.K.; Rodríguez, V.; Ortega, E.; Fernández-Espín, V.; Janiak, C.; Glazer, E.C.; Barone, G.; et al. Organoplatinum(II) Complexes Self-Assemble and Recognize AT-Rich Duplex DNA Sequences. *Inorg. Chem.* **2021**, *60*, 2178–2187. [CrossRef]
17. Veclani, D.; Tolazzi, M.; Cerón-Carrasco, J.P.; Melchior, A. Intercalation Ability of Novel Monofunctional Platinum Anticancer Drugs: A Key Step in Their Biological Action. *J. Chem. Inf. Model.* **2021**, *61*, 4391–4399. [CrossRef]
18. Wang, F.-Y.; Liu, R.; Huang, K.-B.; Feng, H.-W.; Liu, Y.-N.; Liang, H. New Platinum(II)-Based DNA Intercalator: Synthesis, Characterization, and Anticancer Activity. *Inorg. Chem. Commun.* **2019**, *105*, 182–187. [CrossRef]
19. Pages, B.J.; Garbutcheon-Singh, K.B.; Aldrich-Wright, J.R. Platinum Intercalators of DNA as Anticancer Agents. *Eur. J. Inorg. Chem.* **2017**, *2017*, 1613–1624. [CrossRef]
20. Arabi, A.; Cogley, M.O.; Fabrizio, D.; Stitz, S.; Howard, W.A.; Wheeler, K.A. Anticancer Activity of Nonpolar $Pt(CH_3)_2I_2\{bipy\}$ is Found to be Superior among Four Similar Organoplatinum(IV) Complexes. *J. Mol. Struct.* **2023**, *1274*, 134551. [CrossRef]
21. Engel, L.W.; Young, N.A.; Tralka, T.S.; Lippman, M.E.; O'Brien, S.J.; Joyce, M.J. Establishment and Characterization of Three New Continuous Cell Lines Derived from Human Breast Carcinomas. *Cancer Res.* **1978**, *38*, 3352–3364. [PubMed]
22. O'Brien, A.M.; Wheeler, K.A.; Howard, W.A. Synthesis, Structure, and Anticancer Activity of a Dinuclear Organoplatinum(IV) Complex Stabilized by Adenine. *Compounds* **2025**, *5*, 16. [CrossRef]
23. Clark, H.C.; Manzer, L.E. Reactions of π-(1,5-Cyclooctadiene)organoplatinum(II) Compounds and the Synthesis of Perfluoroalkylplatinum Complexes. *J. Organomet. Chem.* **1973**, *59*, 411–428. [CrossRef]
24. Appleton, T.G. *Encyclopedia of Spectroscopy and Spectrometry*, 3rd ed.; Academic Press: Cambridge, MA, USA, 2017.
25. Sheldrick, G.M. *SADABS and TWINABS—Program for Area Detector Absorption Corrections*; University of Göttingen: Göttingen, Germany, 2014.

26. Barbour, L.J. X-Seed 4: Updates to a Program for Small-Molecule Supramolecular Crystallography. *J. Appl. Cryst.* **2020**, *53*, 1141–1146. [CrossRef]
27. Sheldrick, G.M. SHELXT-Integrated Space-Group and Crystal-Structure Determination. *Acta Cryst. A* **2015**, *71*, 3–8. [CrossRef]
28. Kumar, C.V.; Asuncion, E.H. DNA Binding Studies and Site Selective Fluorescence Sensitization of an Anthryl Probe. *J. Am. Chem. Soc.* **1993**, *115*, 8547–8553. [CrossRef]
29. Morris, J.; Kunkel, M.W.; White, S.L.; Wishka, D.G.; Lopez, O.D.; Bowles, L.; Brady, P.S.; Ramsey, P.; Grams, J.; Rohrer, T.; et al. Targeted Investigational Oncology Agents in the NCI60: A Phenotypic Systems-Based Resource. *Mol. Cancer Ther.* **2023**, *22*, 1270–1279. [CrossRef]
30. Shoemaker, R.H. The NCI60 Human Tumor Cell Line Anticancer Drug Screen. *Nat. Rev. Cancer* **2006**, *6*, 813–823. [CrossRef]
31. Monks, A.; Scudiero, D.; Skehan, P.; Shoemaker, R.; Paull, K.; Vistica, D.; Hose, C.; Langley, J.; Cronise, P.; Vaigro-Wolff, A.; et al. Feasibility of a High-Flux Anticancer Drug Screen Using a Diverse Panel of Cultured Human Tumor Cell Lines. *J. Natl. Cancer Inst.* **1991**, *83*, 757–766. [CrossRef]
32. D'Abramo, M.; Castellazzi, C.L.; Orozco, M.; Amadei, A. On the Nature of DNA Hyperchromic Effect. *J. Phys. Chem. B* **2013**, *117*, 8697–8704. [CrossRef]
33. Tu, B.; Chen, Z.-F.; Liu, Z.-J.; Cheng, L.-Y.; Hu, Y.-J. Interaction of Flavones with DNA in Vitro: Structure-Activity Relationships. *RSC Adv.* **2015**, *5*, 33058–33066. [CrossRef]
34. Brattain, M.G.; Fine, W.D.; Khaled, F.M.; Thompson, J.; Brattain, D.E. Heterogeneity of Malignant Cells from a Human Colonic Carcinoma. *Cancer Res.* **1981**, *41*, 1751–1756.
35. Semple, T.U.; Quinn, L.A.; Woods, L.K.; Moore, G.E. Tumor and Lymphoid Cell Lines from a Patient with Carcinoma of the Colon for a Cytotoxicity Model. *Cancer Res.* **1978**, *38*, 1345–1355.
36. Kunkel, M.W.; Coussens, N.P.; Morris, J.; Taylor, R.C.; Dexheimer, T.S.; Jones, E.M.; Doroshow, J.H.; Teicher, B.A. HTS384 NCI60: The Next Phase of the NCI60 Screen. *Cancer Res.* **2024**, *84*, 2403–2416. [CrossRef] [PubMed]
37. Chen, T.R.; Dorotinsky, C.S.; McGuire, L.J.; Macy, M.L.; Hay, R.J. DLD-1 and HCT-15 Cell Lines Derived Separately from Colorectal Carcinomas Have Totally Different Chromosome Changes but the Same Genetic Origin. *Cancer Genet. Cytogenet.* **1995**, *81*, 103–108. [CrossRef] [PubMed]
38. Marshall, C.J.; Franks, L.M.; Carbonell, A.W. Markers of Neoplastic Transformation in Epithelial Cell Lines Derived from Human Carcinomas. *J. Natl. Cancer Inst.* **1977**, *58*, 1743–1751. [CrossRef] [PubMed]
39. Camps, J.; Morales, C.; Prat, E.; Ribas, M.; Capellà, G.; Egozcue, J.; Peinado, M.A.; Miró, R. Genetic Evolution in Colon Cancer KM12 Cells and Metastatic Derivates. *Int. J. Cancer* **2004**, *110*, 869–874. [CrossRef]
40. Stragand, J.J.; Barlogie, B.; White, R.A.; Drewinko, B. Biological Properties of the Human Colonic Adenocarcinoma Cell Line SW 620 Grown as a Xenograft in the Athymic Mouse. *Cancer Res.* **1981**, *41*, 3364–3369.
41. Boland, C.R.; Goel, A. Microsatellite Instability in Colorectal Cancer. *Gastroenterology* **2010**, *138*, 2073–2087. [CrossRef]
42. Koi, M.; Umar, A.; Chauhan, D.P.; Cherian, S.P.; Carethers, J.M.; Kunkel, T.A.; Boland, C.R. Human Chromosome 3 Corrects Mismatch Repair Deficiency and Microsatellite Instability and Reduces N-Methyl-N′-nitro-N-nitrosoguanidine Tolerance in Colon Tumor Cells with Homozygous *hMLH1* Mutation. *Cancer Res.* **1994**, *54*, 4308–4312.
43. Foley, G.E.; Lazarus, H.; Farber, S.; Uzman, B.G.; Boone, B.A.; McCarthy, R.E. Continuous Culture of Human Lymphoblasts from Peripheral Blood of a Child with Acute Leukemia. *Cancers* **1965**, *18*, 522–529. [CrossRef]
44. Birnie, G.D. The HL60 Cell Line: A Model System for Studying Human Myeloid Cell Differentiation. *Br. J. Cancer* **1988**, *58*, 41–45.
45. Greenberg, J.M.; Gonzalez-Sarmiento, R.; Arthur, D.C.; Wilkowski, C.W.; Streifel, B.J.; Kersey, J.H. Immunophenotypic and Cytogenetic Analysis of Molt-3 and Molt-4: Human T-Lymphoid Cell Lines with Rearrangement of Chromosome 7. *Blood* **1988**, *72*, 1755–1760. [CrossRef]
46. Matsuoka, Y.; Moore, G.E.; Yagi, Y.; Pressman, D. Production of Free Light Chains of Immunoglobulin by a Hematopoietic Cell Line Derived from a Patient with Multiple Myeloma. *Proc. Soc. Exp. Biol. Med.* **1967**, *125*, 1246–1250. [CrossRef]
47. Yang, S.; Damiano, M.G.; Zhang, H.; Tripathy, S.; Luthi, A.J.; Rink, J.S.; Ugolkov, A.V.; Singh, A.T.K.; Dave, S.S.; Gordon, L.I.; et al. Biomimetic, Synthetic HDL Nanostructures for Lymphoma. *Proc. Natl. Acad. Sci. USA* **2013**, *110*, 2511–2516. [CrossRef]
48. Wang, Y.; Dai, Z.; Sadee, W.; Hancock, W.S. A Pharmacoproteomics Study of the Cancer Cell Line EKVX Using Capillary-LC/MS/MS. *Mol. Pharm.* **2006**, *3*, 566–578. [CrossRef]
49. Zhang, H.; Li, N.; Chen, Y.; Huang, L.-Y.; Wang, Y.-C.; Fang, G.; He, D.-C.; Xiao, X.-Y. Protein Profile of Human Lung Squamous Carcinoma Cell Line NCI-H226. *Biomed. Eng. Sci.* **2007**, *20*, 24–32.
50. Shi, Y.; Fu, X.; Hua, Y.; Han, Y.; Lu, Y.; Wang, J. The Side Population in Human Lung Cancer Cell Line NCI-H460 Is Enriched in Stem-Like Cancer Cells. *PLoS ONE* **2012**, *7*, e33358. [CrossRef]
51. Gazdar, A.F.; Minna, J.D. NCI Series of Cell Lines: An Historical Perspective. *J. Cell. Biochem. Suppl.* **1996**, *24*, 1–11. [CrossRef] [PubMed]
52. Rutka, J.T.; Giblin, J.R.; Høifødt, H.K.; Dougherty, D.V.; Bell, C.W.; McCulloch, J.R.; Davis, R.L.; Wilson, C.B.; Rosenblum, M.L. Establishment and Characterization of a Cell Line from a Human Gliosarcoma. *Cancer Res.* **1986**, *46*, 5893–5902.

53. Torsvik, A.; Stieber, D.; Enger, P.Ø.; Golebiewska, A.; Molven, A.; Svendsen, A.; Westermark, B.; Niclou, S.P.; Olsen, T.K.; Enger, M.C.; et al. U-251 Revisited: Genetic Drift and Phenotypic Consequences of Long-Term Cultures of Glioblastoma Cells. *Cancer Med.* **2014**, *3*, 812–824. [CrossRef]
54. Fogh, J.; Fogh, J.M.; Orfeo, T. One Hundred and Twenty-Seven Cultured Human Tumor Cell Lines Producing Tumors in Nude Mice. *J. Natl. Cancer Inst.* **1977**, *59*, 221–226. [CrossRef]
55. Sustarsic, E.G.; Junnila, R.K.; Kopchick, J.J. Human Metastatic Melanoma Cell Lines Express High Levels of Growth Hormone Receptor and Respond to GH Treatment. *Biochem. Biophys. Res. Commun.* **2013**, *441*, 144–150. [CrossRef]
56. Bénard, J.; Da Silva, J.; De Blois, M.-C.; Boyer, P.; Duvillard, P.; Chiric, E.; Riou, G. Characterization of a Human Ovarian Adenocarcinoma Line, IGROV1, in Tissue Culture and in Nude Mice. *Cancer Res.* **1985**, *45*, 4970–4979. [PubMed]
57. Hamilton, T.C.; Young, R.C.; McKoy, W.M.; Grotzinger, K.R.; Green, J.A.; Chu, E.W.; Whang-Peng, J.; Rogan, A.M.; Green, W.R.; Ozols, R.F. Characterization of Human Ovarian Carcinoma Cell Line (NIH:OVCAR-3) with Androgen and Estrogen Receptors. *Cancer Res.* **1983**, *43*, 5379–5389.
58. Nunes, M.; Silva, P.M.A.; Coelho, R.; Pinto, C.; Resende, A.; Bousbaa, H.; Almeida, G.M.; Ricardo, S. Generation of Two Paclitaxel-Resistant High-Grade Serous Carcinoma Cell Lines with Increased Expression of P-Glycoprotein. *Front. Oncol.* **2021**, *11*, 752127. [CrossRef]
59. Kaighn, M.E.; Narayan, K.S.; Ohnuki, Y.; Lechner, J.F.; Jones, L.W. Establishment and Characterization of a Human Prostatic Carcinoma Cell Line (PC-3). *Investig. Urol.* **1979**, *17*, 16–23.
60. Neve, R.M.; Chin, K.; Fridlyand, J.; Yeh, J.; Baehner, F.L.; Fevr, T.; Clark, L.; Bayani, N.; Coppe, J.-P.; Tong, F.; et al. A Collection of Breast Cancer Cell Lines for the Study of Functionally Distinct Cancer Subtypes. *Cancer Cell* **2006**, *10*, 515–527. [CrossRef]
61. Mitra, A.K.; Davis, D.A.; Tomar, S.; Roy, L.; Gurler, H.; Xie, J.; Lantvit, D.D.; Cardenas, H.; Fang, F.; Liu, Y.; et al. In Vivo Tumor Growth of High-Grade Serous Ovarian Cancer Cell Lines. *Gynecol. Oncol.* **2015**, *138*, 372–377. [CrossRef]
62. Vert, A.; Castro, J.; Ribó, M.; Vilanova, M.; Benito, A. Transcriptional Profiling of NCI/ADR-RES Cells Unveils a Complex Network of Signaling Pathways and Molecular Mechanisms of Drug Resistance. *OncoTargets Ther.* **2018**, *11*, 221–237. [CrossRef]
63. Nakatsuka, E.; Tan, L.; Cunneen, B.; Foster, C.; Lei, Y.L.; McLean, K. Characterization of DNA Damage Repair Pathway Utilization in High-Grade Serous Ovarian Cancers Yields Rational Therapeutic Approaches. *Transl. Oncol.* **2024**, *50*, 102119. [CrossRef] [PubMed]
64. Meijer, T.G.; Martens, J.W.M.; Prager-van der Smissen, W.J.C.; Verkaik, N.S.; Beaufort, C.M.; van Herk, S.; Robert-Finestra, T.; Hoogenboezem, R.M.; Ruigrok-Ritstier, K.; Paul, M.W.; et al. Functional Homologous Recombination (HR) Screening Shows the Majority of BRCA1/2-Mutant Breast and Ovarian Cancer Cell Lines Are HR-Proficient. *Cancers* **2024**, *16*, 741–758. [CrossRef] [PubMed]
65. Štarha, P.; Vančo, J.; Trávníček, Z. Platinum Iodo Complexes: A Comprehensive Overview of Anticancer Activity and Mechanisms of Action. *Coord. Chem. Rev.* **2019**, *380*, 103–135. [CrossRef]

Disclaimer/Publisher's Note: The statements, opinions and data contained in all publications are solely those of the individual author(s) and contributor(s) and not of MDPI and/or the editor(s). MDPI and/or the editor(s) disclaim responsibility for any injury to people or property resulting from any ideas, methods, instructions or products referred to in the content.